Journal of Power Sources 268 (2014) 37–44

Contents lists available at ScienceDirect

Journal of Power Sources

journal homepage: www.elsevier.com/locate/jpowsour

Improved electrolyte and its application in $LiNi_{1/3}Mn_{1/3}Co_{1/3}O_2$—Graphite full cells

Minghong Liu [a], Fang Dai [b], Zhiru Ma [c], Marty Ruthkosky [d], Li Yang [d, *]

[a] Shenzhen BAK Technology Co., Ltd, China
[b] Optimal CAE, United States
[c] Corporate Analytical, WR Grace, United States
[d] Chemical and Materials Systems Laboratory, General Motors Corporation, Warren 48090, United States

HIGHLIGHTS

- High temperature stable electrolyte has been developed.
- Detailed study of LiODFB additive has been conducted with DFT calculations.
- LiODFB added electrolyte show better capacity retention for NMC—Graphite cell at 60 °C.

ARTICLE INFO

Article history:
Received 22 March 2014
Received in revised form
30 April 2014
Accepted 20 May 2014
Available online 9 June 2014

Keywords:
Lithium
NMC
Electrolyte
Additives
LiODFB
SEI

ABSTRACT

Lithium oxalatodifluoroborate (LiODFB) has been synthesized and used as a novel electrolyte additive. Standard and modified electrolytes were flame-sealed in NMR tubes and stored at 60 °C for 3 months. Multiple nuclear NMR (^1H, ^{11}B, ^{13}C, ^{19}F, ^{31}P) studies confirmed that the modified electrolyte (2% LiODFB added) showed no signs of decomposition as that of regular electrolyte, which is possibly due to the —F of $LiPF_6$ and oxalate of LiODFB ligand exchange effect. The high temperature stabilization mechanism of the added LiODFB was studied using quantum mechanical calculations. Electrochemical tests of $LiNi_{1/3}Mn_{1/3}Co_{1/3}O_2$ (NMC)—Graphite full-cells with and without LiODFB as the electrolyte additive were conducted. When cycling with the NMC—Graphite full-cell at elevated temperature (60 °C), the 100th cycle capacity retention rate of the modified electrolyte was 60%, compared to 27% with the standard electrolyte. The EIS study indicates the full-cells with LiODFB have much lower interfacial impedance than the standard cells. Theoretical calculations reveal that LiODFB generates a layer of thin and resilient SEI on the graphite surface at a higher reduction potential than ethylene carbonate (EC) due to its higher ring strain and protects graphite from the toxic Mn^{2+} resulting in improved electrochemical performance of NMC—Graphite based cells.

1. Introduction

Lithium-ion batteries (LIBs) are one of the most widely used portable power sources [1]. However, dramatic loss of energy and power at relatively high temperatures (>45 °C), limits the long term application (>10 years) of LIB for electric vehicles (EVs) and hybrid electric vehicles (HEV). The performance degradation of the LIB, besides the cathode and anode materials, is also frequently linked to the thermal instability of $LiPF_6$ and the reactions of the electrolyte with the surface of the electrode materials [2–4].

Due to the irreplaceable and dominant role of $LiPF_6$ as a lithium salt electrolyte, scientists over the world are doing extensive research on electrolyte additives which can stabilize the $LiPF_6$ based electrolyte at elevated temperature. For example, the —N related additives, dimethyl acetamide (DMAc) and N-methyl-2-pyrrolidone (NMP) [4,5], used by Dr. B. Lucht and the -P atom based additives, phosphate and phosphonate [6,7], discovered by Dr. S.S. Zhang and Dr. K. Xu can all stabilize the $LiPF_6$ based electrolyte by forming the Lewis base (additive) —Lewis acid (PF_5) complex.

Another extensive research area is on SEI precursors that can protect the graphite from exfoliation by suppressing the co-intercalation of solvent molecules. The most successful case is the substitution of propylene carbonate (PC) with ethylene carbonate (EC) which makes the LIB commercially viable [8]. Furthermore,

* Corresponding author. Tel.: +1 586 947 0153.
E-mail addresses: li.1.yang@gm.com, lyang27@gmail.com (L. Yang).

http://dx.doi.org/10.1016/j.jpowsour.2014.05.109
0378-7753/

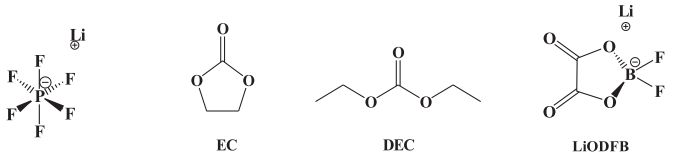

Scheme 1. The structure of the standard electrolyte and LiODFB.

some other chemicals, especially the five-membered ring based species, such as vinyl carbonate (VC) [9–11], vinyl ethylene carbonate (VEC) [12,13], 1,3-propanesultone (PS) [14] and lithium bis(oxalato)borate (LiBOB) [15] has been discovered to form a more stable and resilient SEI so as to improve the electrochemical performance of LIBs. LiODFB which shares structural elements of both LiBOB and $LiBF_4$, also belongs to this category.

Of all these electrolyte additives, LiBOB and LiODFB are the ones which have bi-functionality, to stabilize the electrolyte at elevated temperature [16,17] and help form a stable SEI. In this report, LiODFB has been synthesized in our lab and the modified electrolyte with 2% LiODFB has been tested for both thermal storage performance and electrochemical performance with the $LiNi_{1/3}Mn_{1/3}Co_{1/3}O_2$(NMC)—Graphite full-cell. Also, theoretical calculations have been conducted for a better understanding of the additive's functions as $LiPF_6$ stabilizer and SEI precursor.

2. Experimental

Lithium oxalatodifluoroborate (LiODFB) was synthesized by reacting lithium oxalate with boron trifluoride-etherate (BF_3-DEE),

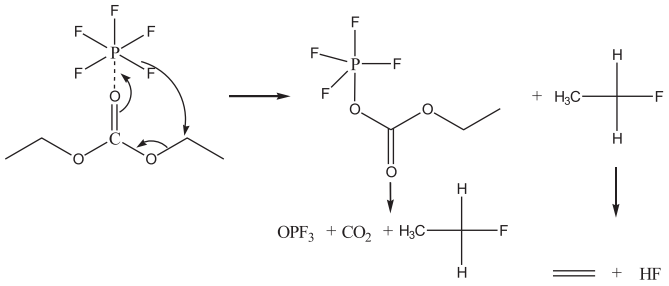

Scheme 2. The decomposition mechanism of DEC.

followed by re-crystallization from dimethyl carbonate (DMC) at 0 °C to remove $LiBF_4$ [18]. The standard electrolyte, 1 M $LiPF_6$-EC: Diethyl carbonate (DEC) (1:2, v:v) electrolyte was purchased from Novolyte, Inc. The modified electrolyte was prepared by adding 2% (wt.%) LiODFB into the standard electrolyte. $LiNi_{1/3}Mn_{1/3}Co_{1/3}O_2$ (NMC) is acquired from Toda America and the graphite anode was obtained from Timcal Graphite & Carbon Company.

Fourier Transform Infrared-Attenuated Total Reflectance (FTIR-ATR) measurements of lithium salts were obtained on a Thermo Nicolet iS10 IR spectrometer equipped with a Smart Performer accessory with a Germanium crystal. For each sample, 128 scans were collected and purged with high purity argon during the entire experiment.

The ^1H, ^{13}C, ^{11}B, ^{19}F and ^{31}P NMR data were collected on liquid samples with a Bruker 500 MHz NMR spectrometer at Michigan State University (MSU). ^1H and ^{13}C NMR resonances were referenced to TMS at 0 ppm, ^{11}B NMR resonances were referenced to BF_3

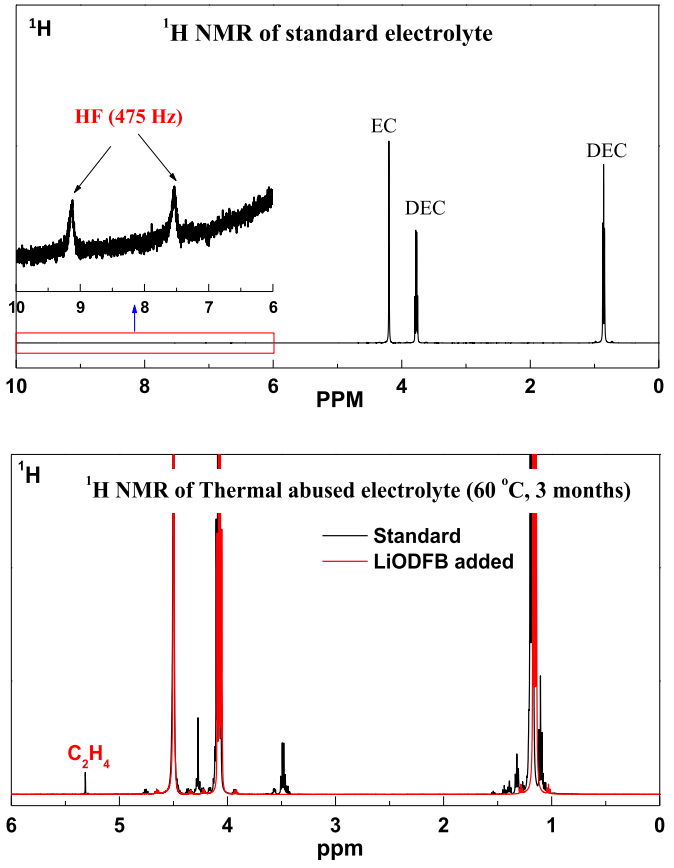

Fig. 1. ^1H NMR spectra of fresh standard electrolyte (up) & thermally abused electrolytes (down).

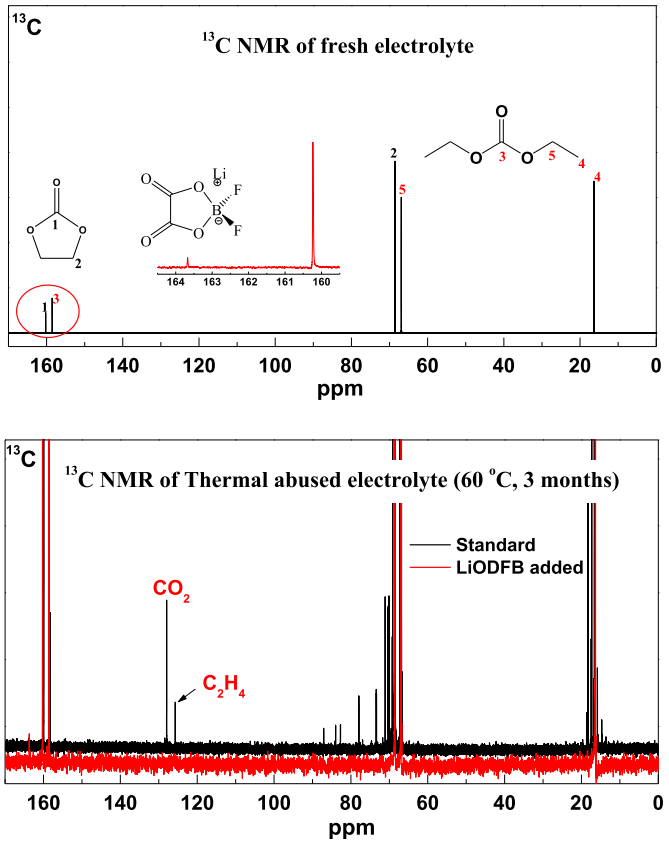

Fig. 2. ^{13}C NMR spectra of fresh electrolyte (up) & thermally abused electrolytes (down).

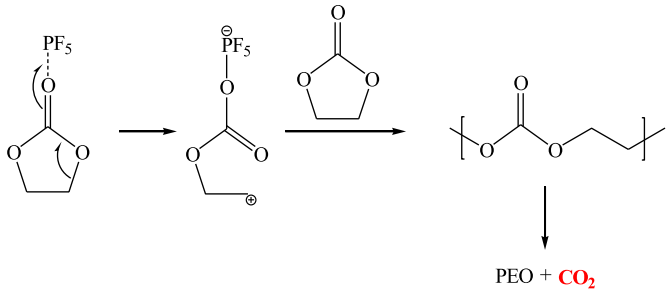

Scheme 3. The decomposition mechanism of EC.

$O(C_2H_5)$ at 0 ppm. ^{19}F and ^{31}P NMR resonances were referenced to $LiPF_6$ at −74.5 ppm and $LiPF_6$ at −145 ppm, respectively.

Electrochemical testing (cycling and EIS) of the cells were conducted with VMP3 Electrochemical Workstation from Bio-Logic. Full-cells (NMC–Graphite) and half-cells based on 2032 type coin-cells were fabricated and activated by 1 cycle at 1/20C and 2 cycles at 1/10C, and cycled ~100 times at 1/2C at 30 °C or 60 °C. House-made 3-electrode coin cells were fabricated with lithium metal as a reference electrode to check the voltage profile. Electrochemical Impedance Spectroscopy (EIS) analyses of the coin cells were performed at 30 °C, sweeping from 100 KHz to 0.1 Hz with an AC perturbation amplitude of 10 mV.

DFT calculations were performed with the Firefly QC package [19], which is partially based on the GAMESS (US) source code [20]. Geometries (gas phase) of all of the molecules selected in this study were fully optimized by using Density Functional Theory (DFT) and B3LYP method, with 6–31G (d) basis set. Also B3LYP method with 6–311 + G (2d,p) basis set was used for single energy calculation based on the optimized geometries.

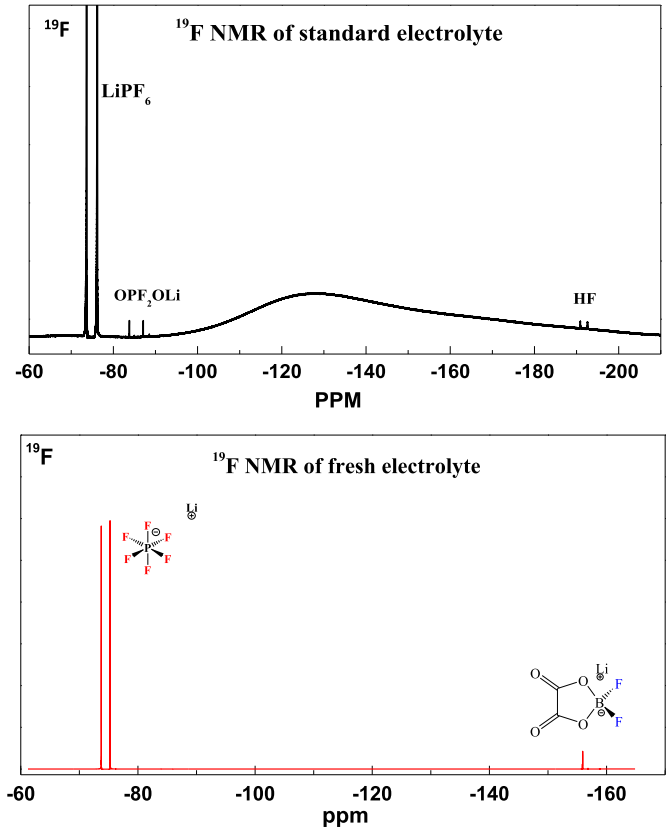

Fig. 3. ^{19}F NMR spectra of fresh electrolytes without (up) & with LiODFB (down).

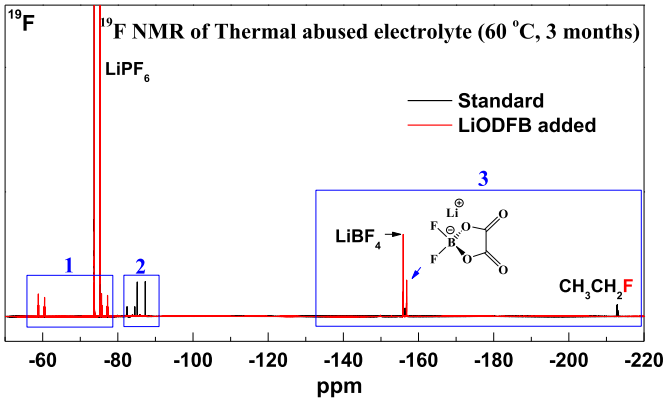

Fig. 4. ^{19}F NMR spectra of thermally abused electrolytes (overview).

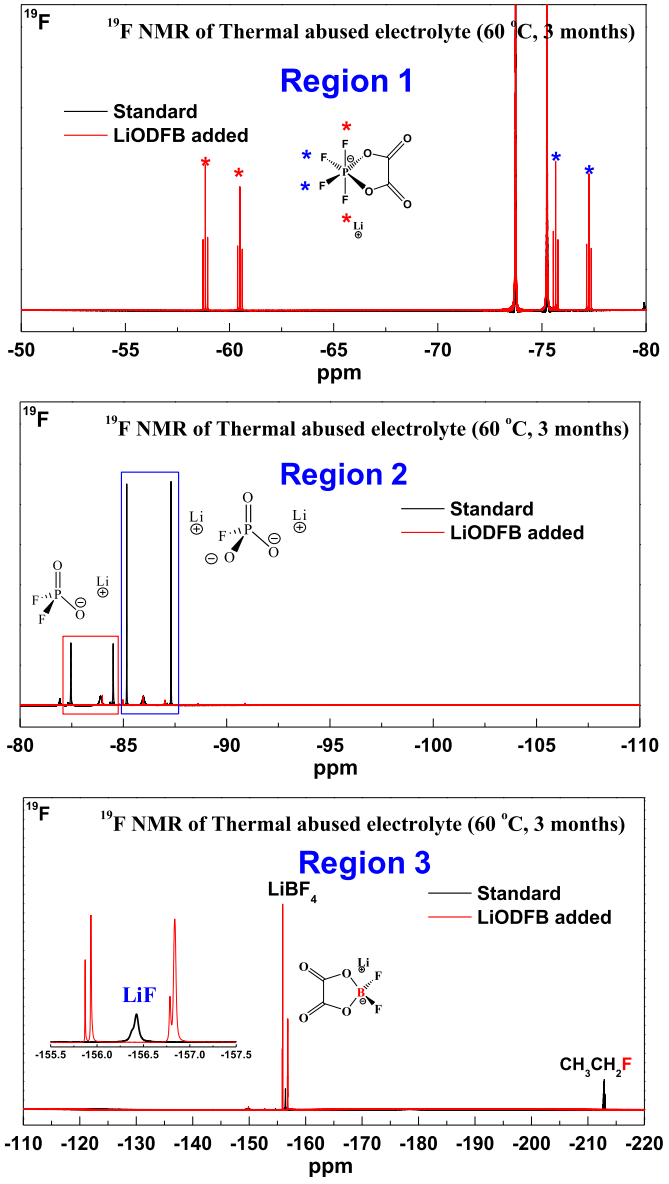

Fig. 5. ^{19}F NMR spectra of thermally abused electrolytes (continued).

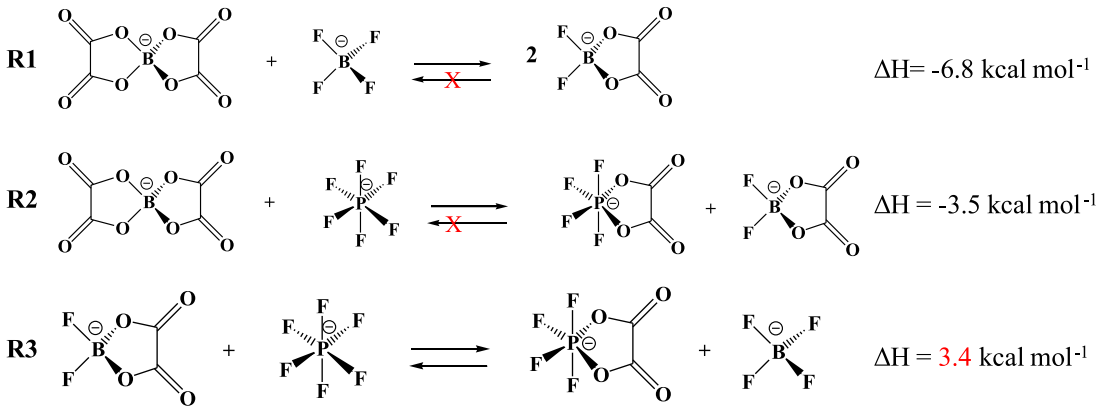

Scheme 4. The calculated enthalpy of ligand exchange.

Scheme 5. The decomposition of $LiPF_6$ at elevated temperatures.

3. Results and discussion

3.1. NMR study of the standard and modified electrolyte, before and after thermal abuse at 60 °C

The chemical structures of standard electrolyte (1.0 M $LiPF_6$ in EC: DEC (1:2, v:v)) are listed in Scheme 1. The modified electrolyte is prepared by adding 2% (wt.%) of LiODFB into the standard electrolyte. The flame sealed NMR tubes with standard and modified electrolyte are stored at 60 °C for several months, with discoloration of the standard electrolyte to dark brown while the LiODFB added one remains clean and clear.

3.1.1. ^{1}H of the electrolyte

^{1}H NMR spectra of the fresh and thermally abused electrolytes are shown in Fig. 1. From the thermal abused ^{1}H NMR (down), it is clear that the standard electrolyte (black line) decomposed and generated C_2H_4 (5.3 ppm) after storage at 60 °C for 3 months. Other non-resolved peaks for the standard electrolyte (1.5 ppm, 3.5 ppm and 4.3 ppm) are the products of EtF and ether oligomers.

The modified electrolyte (red line), however, maintains a clean ^{1}H NMR spectrum and no such decomposition products were detected with the exception of some tiny ^{13}C satellites bands around EC and DEC. The detailed decomposition mechanism of the DEC without additive is listed in Scheme 2 [21].

3.1.2. ^{13}C of the electrolyte

^{13}C NMR spectrum of the fresh, modified electrolytes, together with thermal abused electrolytes are listed in Fig. 2. For standard electrolyte, strong C_2H_4 and CO_2 signals has been detected Fig. 2 (down, black line) after thermal abuse, due to the decomposition of DEC. Furthermore, EC also underwent polymerization with the catalytic effect of PF_5 to form polyethylene carbonate (PEC) releasing CO_2 and forming polyethers/oligermers (Scheme 3), shown by the peaks around 70 ppm, typical of ethereal carbons [22].

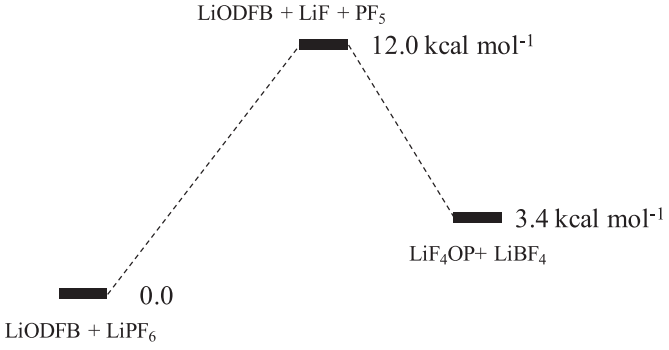

Scheme 7. Detailed reaction route of LiODFB with $LiPF_6$.

3.1.3. ^{19}F of the electrolyte

^{19}F NMR spectrum of the fresh and modified electrolyte is listed in Fig. 3. The symmetric doublet at −74 ppm is the fluorine signal of $LiPF_6$ which is split by the neighboring ^{31}P nuclei. For the standard electrolyte, the small quantity of OPF_2OLi (−85.5 ppm) and HF (−191.8 ppm) is also detected. For the modified electrolyte, the −F signal of LiODFB is located at −155.5 ppm.

^{19}F NMR spectrum of the thermally abused standard electrolyte (all ranges, from −50 ppm to −200 ppm) are listed in Fig. 4. Three regions (1,2 and 3) are divided and will be discussed next.

Region 1 (Fig. 5, up) shows a doublet at −59.7 ppm and a triplet at −76.5 ppm indicating the formation of lithium tetrafluoro oxolato phosphate (LiF_4OP) [16] resulting from the exchange of the −F and

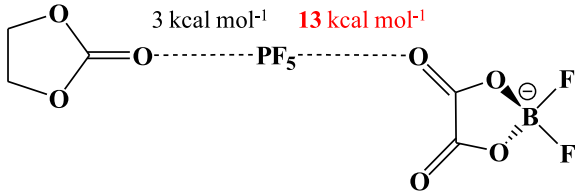

Scheme 8. Binding energies of EC—PF_5 and ODFB—PF_5.

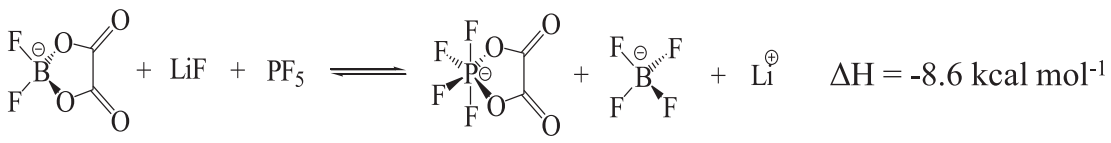

Scheme 6. The modified enthalpy of LiODFB reacting with PF_5 and LiF.

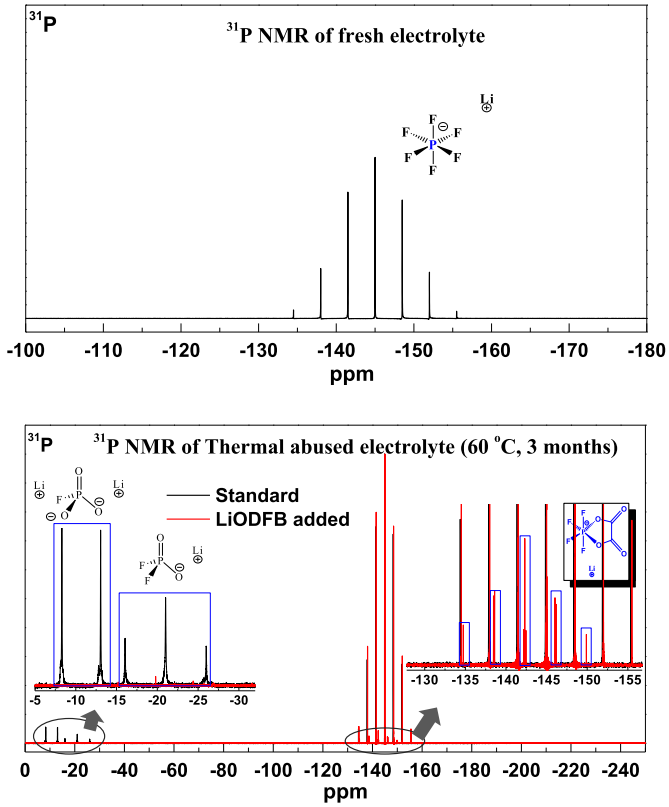

Fig. 6. ^{31}P NMR spectra of fresh electrolyte (up) & thermally abused electrolytes (down).

oxalato ligands from $LiPF_6$ and LiODFB. Additionally, information on ligand exchanges and calculated enthalpies for LiBOB, $LiBF_4$, LiODFB and $LiPF_6$ are listed in Scheme 4. From the data, we can see that it is thermally favorable for the reaction of LiBOB with $LiBF_4$ or $LiPF_6$ to generate the LiODFB and LiF_4OP (R1 and R2), and is not thermally favorable for the reaction of LiODFB with $LiPF_6$ (R3), even considering the entropy effect (entropy is slightly increasing and not listed here). The key for this major difference is in the thermal instability of $LiPF_6$ which leads to its decomposition to PF_5 and LiF, as listed in Schemes 5 and 6. This endothermic reaction basically increases the system energy of the LiODFB, PF_5 and LiF and forms the less active lithium salt mixture, LiF_4OP and $LiBF_4$ and is the reason for the stabilizing effect of the LiODFB on the $LiPF_6$ based electrolyte. This mechanism is similar to the decomposition of EC or DEC when coordinating with PF_5 to release the deleterious HF, C_2H_4, CO_2, EtF and ether oligomers, etc (as listed in Scheme 2 and Scheme 3). However, the decomposition of LiODFB coordinating with PF_5 (together with LiF) generates benign products such as $LiBF_4$ and LiF_4OP, which are harmless to the overall electrochemical performance. The decomposition mechanism of LiODFB is different from the Lewis acid-base mechanism such as DMAc—PF_5 as mentioned before, in which DMAc does not decompose. Scheme 7 gives a detailed reaction path for the system stabilizing reaction 3 (R3).

Further analysis of the reaction of LiBOB and $LiBF_4$ to generate LiODFB (R1, Scheme 4), indicates the reaction is not reversible, i.e. LiODFB will not spontaneously form LiBOB and $LiBF_4$. This hypothesis is also confirmed in the recent publication by Dr. Lucht [17], in which only tiny LiBOB and $LiBF_4$ was generated when thermal abuse of the LiODFB in EC:EMC (3:7, v:v) at 100 °C. Furthermore, we predict the reaction (R2) of LiBOB and $LiPF_6$ to generate LiF_4OP and LiODFB is also irreversible, based on similar reason. Conversely, reaction 3 (R3) is reversible due to the non-thermally stable $LiPF_6$ and $LiBF_4$.

Finally, the binding energy of EC—PF_5 and ODFB—PF_5 were also calculated and from Scheme 8, it is clear that the higher binding energy of ODFB—PF_5 (~13 kal mol^{-1}) suppresses the attack of PF_5 on EC and DEC solvent molecules, as shown in Schemes 2 and 3.

In region 2, (−80 ppm to −90 ppm) there are two intense doublets around −83.5 ppm and −86.4 ppm for the standard electrolyte which are attributed to the $Li_xPF_yO_z$ ($LiPF_2O_2$ and Li_2PFO_3) [2], the decomposed products of $LiPF_6$ with trace moisture. Not surprisingly, the modified electrolyte, shows no such decomposition of lithium salts due to the LiODFB stabilizing effect.

In the region 3, (−130 ppm to −220 ppm) there are LiF and EtF decomposition species shown for the standard electrolyte as

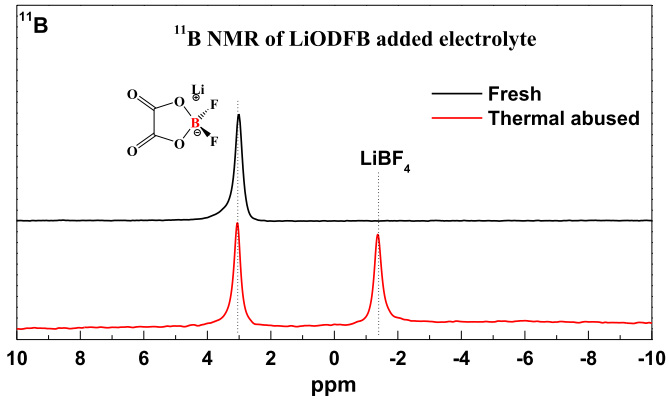

Fig. 7. ^{11}B NMR spectra of the modified electrolyte.

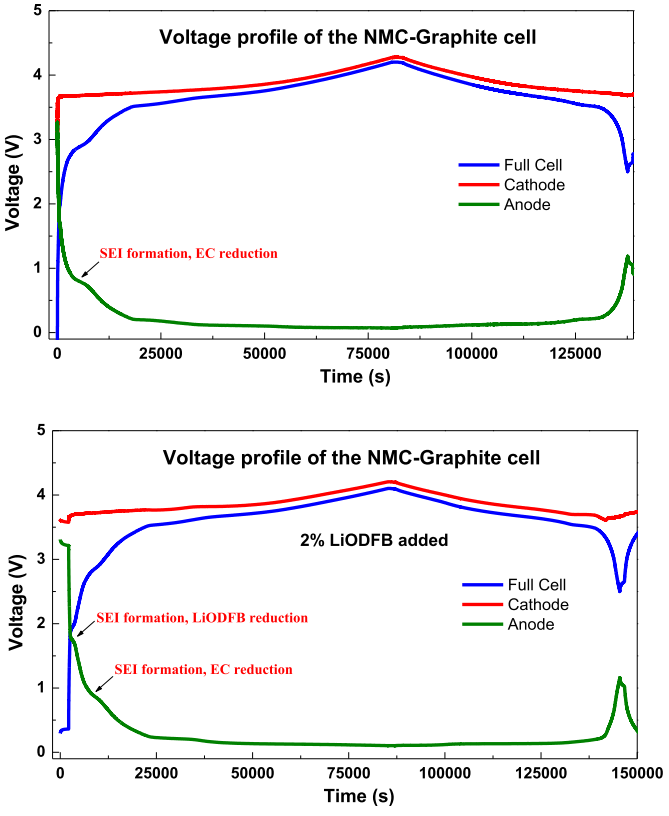

Fig. 8. Voltage profile of NMC–Graphite cell with standard (up) & modified electrolyte (down).

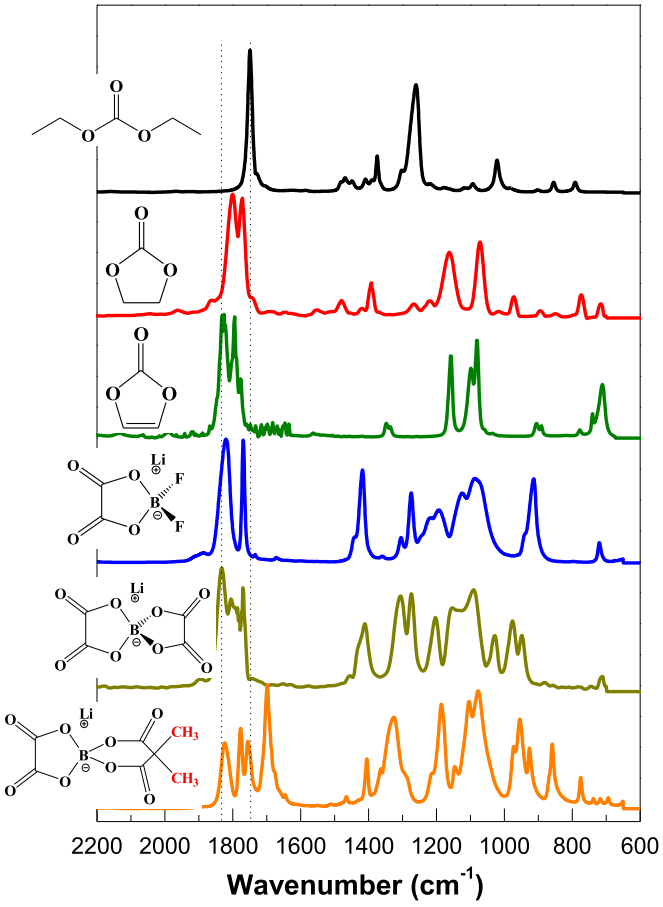

Fig. 9. FTIR spectra of DEC, EC, VC, LiODFB, LiBOB and LiMOB.

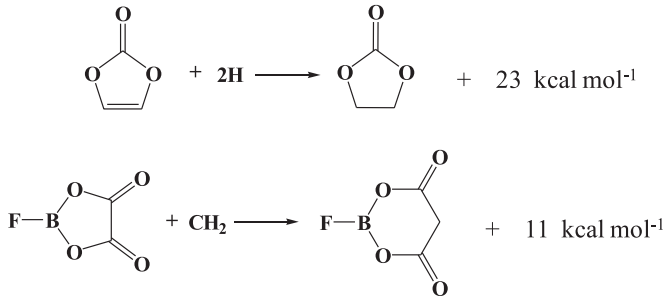

Scheme 11. Calculated ring strains of selected structure.

proposed by the mechanism in Scheme 2 [2]. HF reacts with Li^+ to generate the more stable LiF which precipitates out from the electrolyte. For the modified electrolyte, we can clearly detect the LiODFB and $LiBF_4$ due to the ligands exchange effect, with no signs of LiF and EtF.

3.1.4. *^{31}P of the electrolyte*

The ^{31}P spectrum of the standard electrolyte and thermal abused electrolytes with/without LiODFB is shown in Fig. 6, whereas a septet (7 peaks) at −145 ppm, indicates a -P atom connecting with six -F atoms.

Thermally abused electrolytes show strong signals of $Li_xPF_yO_z$ ($LiPF_2O_2$ and Li_2PFO_3) for the standard electrolyte (down, black) which are at trace levels for the modified electrolyte. Detailed reaction route is listed in scheme 9 [2]. Also, LiF_4OP is detected for LiODFB added electrolyte (down, red), which is in agreement with the ^{19}F NMR.

3.1.5. *^{11}B of the modified electrolyte*

Fig. 7 shows the ^{11}B NMR spectra of the modified electrolyte, before and after thermal abuse. The fresh one shows a peak at 3 ppm which is the boron signal of the LiODFB [17]. After thermal abuse, a new peak appears at −1.7 ppm which is assigned to $LiBF_4$,

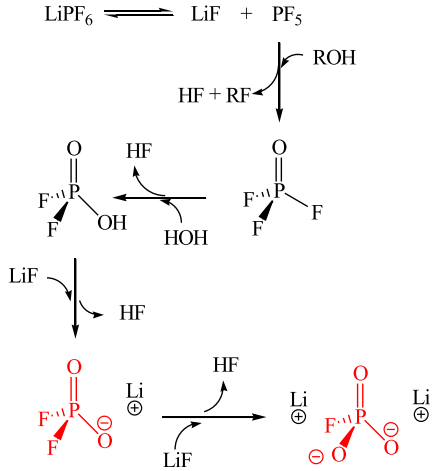

Scheme 9. Decomposition of $LiPF_6$ with moisture.

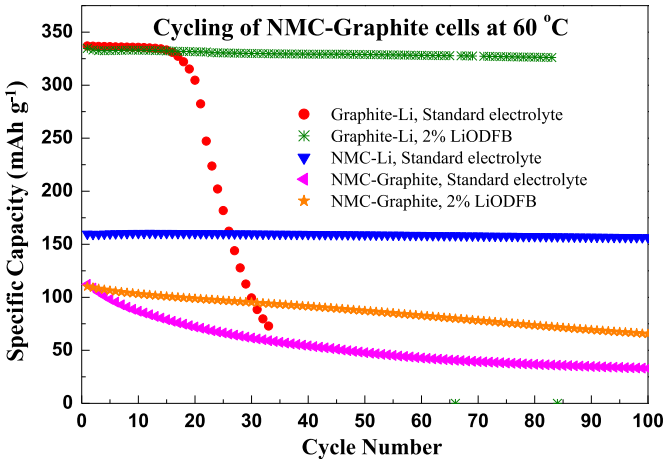

Fig. 10. Cycling of NMC–Graphite cells at 60 °C.

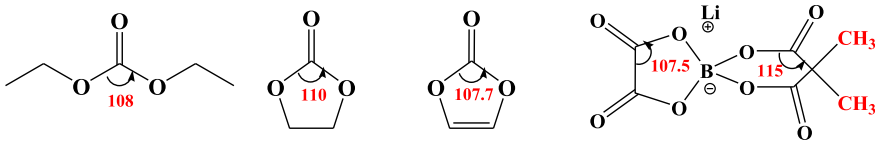

Scheme 10. Calculated bond angles.

as in accordance with the ^{19}F NMR spectra and the ligands exchange mechanism listed in Scheme 6.

3.2. Voltage profile of the NMC–Graphite with/without additives

3-electrode coin cells were built with lithium metal as the reference electrode. The first charge–discharge voltage profiles of the cell with standard and modified electrolyte are shown in Fig. 8. For standard electrolyte, there is a plateau around 0.8 V vs. Li/Li^+ of the graphite anode, due to the reduction of EC, to form a layer of Solid Electrolyte Interphase (SEI) [23,24]. For the modified electrolyte, besides the EC reduction at ~0.8 V, there is another short plateau at ~1.75 V, due to the reduction of LiODFB, as described in the former publication [18]. The reduction mechanism of EC and LiODFB, will be further elaborated in the following part.

3.3. Ring strain of ring structured carbonates and lithium salts

Fig. 9 displays the FTIR spectra of pure DEC, EC, VC, LiODFB, LiBOB and LiMOB. It can be seen that for the ring strained chemicals, the C=O stretching increases to higher wave number, from 1750 cm^{-1} of DEC to 1800 cm^{-1} of EC and 1830 cm^{-1} of VC, LiODFB and LiBOB, etc.

Scheme 10 lists typical calculated sp^2 (120°) hybridization carbon carbonyl (>C=O) bond angles. Typically, five-membered ring structures possess higher ring strain than six-membered rings and other open structures and are less stable. As ring strain increases, the angle between O–C–O (O–C–C) decreases, which forces the carbonyl carbon hybridized orbitals to have more p-orbital character (sp^3 hybridization, 109° 28′) [25]. Considering the total electron density on carbon conservation rule, the carbon connecting with the carbonyl oxygen (=O) has more s-orbital character, and is thus more electronegative. This increasing electronegativity of carbon towards the carbonyl oxygen (=O) concentrates more of the electron cloud from the =O and increases the double bond character of the C=O, shifting the C=O stretching vibration to a higher wave number, as FTIR spectrum (Fig. 9) shows. As for DEC, the electron donating effect of the ethyl group pushes the electron cloud to =O which decrease the double bond character and thus decrease the stretching frequency, possibly.

In order to quantify the relative ring strain of the selected chemical structure, DFT calculations were performed and Scheme 11 lists relative ring strains for the VC-EC and oxalate-malonate based structures of, 23 kcal mol^{-1} and 11 kcal mol^{-1}, respectively. This higher ring strains result in less electrochemical stability (especially cathodic stability) of these chemicals and results a reduction plateau of 1.75 V, 1.0 V and 0.8 V for LiODFB, VC and EC, respectively [9,10,18,26].

3.4. Cycling performance of the half and full NMC–Graphite cells based on standard electrolyte and modified electrolyte

Cycling performance of the NMC–Graphite full-cell and respective half cells at 60 °C is displayed in Fig. 10. Significant difference can be seen for the graphite-Li half cells with standard and modified electrolyte, in which the standard electrolyte rendered a dramatic capacity decrease after ~20 cycles, while the LiODFB modified electrolyte yielded stable cycling at 60 °C. The benefits of LiODFB can also be observed for the NMC–Graphite full-cell cycled at 60 °C, in which the capacity retention rate is 27% for the standard electrolyte and 60% for the LiODFB modified electrolyte, after 100 cycles at 60 °C.

Fig. 11 shows the improvement in the coulombic efficiency from adding LiODFB into the electrolyte of the NMC–Graphite full-cells cycled at 60 °C. The improvement is noted significantly in the earlier cycles, 98% (LiODFB) vs. 95% for the standard electrolyte at 10th cycle. Room temperature cycling performance of the modified electrolyte will be conducted in the future.

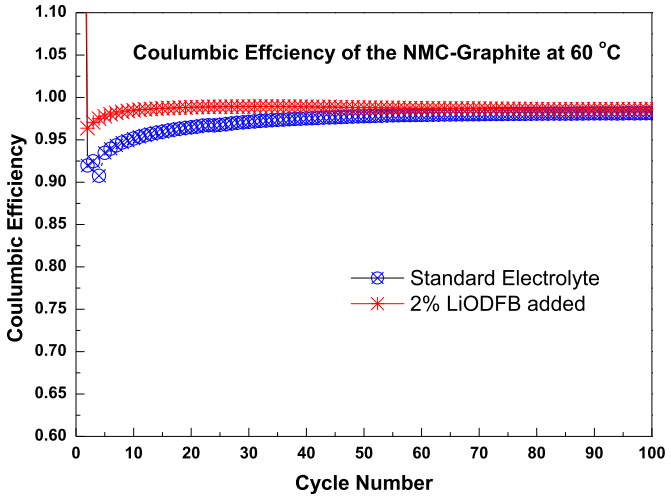

Fig. 11. Columbic efficiency of the NMC–Graphite full-cell at 60 °C.

3.5. EIS analysis of the NMC–Graphite full-cells

EIS of full-cells of standard and modified electrolytes, before and after high temperature cycling, are shown in Fig. 12. The full-cell EIS spectrum is composed of two semi-cycles with a high and low-frequency. The first with a frequency of (>3000 Hz) is attributed to be the electronic conductivity between the active material particles (cathode and anode) and carbon black particles [27]. Both the 60 °C cycled full-cells (with and without additive) show significant high-frequency EIS increase, possibly due to the expanding and shrinking of the electrodes during Li^+ intercalation/deintercalation which results in a loss of electronic contact between the active material particles and carbon black.

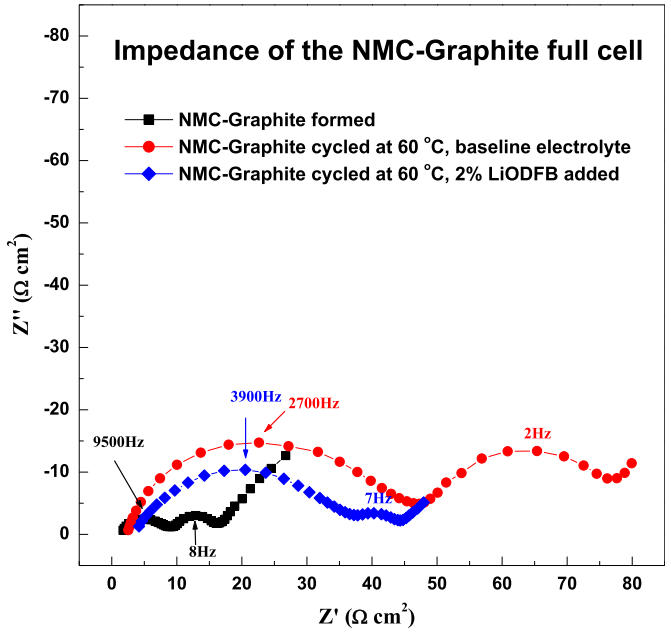

Fig. 12. EIS of full-cells based on standard and modified electrolyte.

The second semi-cycle which has lower frequency (<10 Hz) and is attributed to the interfacial and charge transfer process [27], however, is of significant difference for the cells with standard (30 Ω cm^2) and modified electrolyte (5–8 Ω cm^2). Although a symmetrical cell needs to be built to clarify which electrode (cathode or anode) and to what extent LiODFB contributes to the second semi-cycle, it is believed that the SEI formed on the anode by LiODFB is more stable and resilient [28]. Furthermore, the addition of LiODFB can suppress the electrolyte decomposition at 60 °C, greatly reducing the formation of HF and subsequent attack on NMC and release of toxic Mn^{2+} ions.

4. Conclusion

Lithium oxalatodifluoroborate (LiODFB) has been synthesized and evaluated as an electrolyte additive. In contrast to $LiPF_6$, the LiODFB shows a much improved stability, which is confirmed by thorough studies using variety of nucleus of NMR spectroscopy. The high temperature stabilization mechanism of the LiODFB was also studied using DFT calculations. With the help of the LiODFB, the NMC–Graphite full-cell shows a good capacity retention (60%) at elevated temperature (60 °C), which is much improved than that of standard electrolyte (27%).

Acknowledgment

We thank Dr. Yan Wu for the supplying the NMC cathode, Dr. Xingcheng Xiao for help with the fabrication of coin-cells and Dr. Daniel Holmes at MSU for help with the NMR testing.

References

[1] O. Yamamoto, M. Wakihara, Lithium Ion Batteries: Fundamentals and Performance, Kodansha; Wiley-VCH, Tokyo: Weinheim; New York, 1998, p. 247 xiii.
[2] C.L. Campion, W. Li, B.L. Lucht, J. Electrochem. Soc. 152 (12) (2005) A2327–A2334.
[3] D.P. Abraham, et al., Diagnostic Examination of Generation 2 Lithium-Ion Cells and Assessment of Performance Degradation Mechanisms, 2005.
[4] W. Li, B.L. Lucht, Electrochem. Solid-State Lett. 10 (4) (2007) A115.
[5] M.C. Smart, B.L. Lucht, B.V. Ratnakumar, J. Electrochem. Soc. 155 (8) (2008) A557–A568.
[6] S. Zhang, et al., Electrochem. Solid-State Lett. 4 (12) (2001) A206–A208.
[7] T.R. Jow, S.S.Z., K. Xu, U.S. Patent Application 10/307,537.
[8] R. Fong, U. von Sacken, J.R. Dahn, J. Electrochem. Soc. 137 (7) (1990) 2009–2013.
[9] D. Aurbach, et al., Electrochim. Acta 47 (9) (2002) 1423–1439.
[10] D. Aurbach, et al., J. Electrochem. Soc. 151 (1) (2004) A23–A30.
[11] T. Sasaki, et al., J. Electrochem. Soc. 152 (10) (2005) A2046–A2050.
[12] G. Chen, et al., Electrochem. Solid-State Lett. 8 (7) (2005) A344–A347.
[13] Y. Hu, et al., Electrochem. Solid-State Lett. 7 (11) (2004) A442–A446.
[14] G. Park, et al., J. Power Sources 189 (1) (2009) 602–606.
[15] K. Xu, et al., Electrochem. Solid-State Lett. 5 (11) (2002) A259–A262.
[16] A. Xiao, L. Yang, B.L. Lucht, Electrochem. Solid-State Lett. 10 (11) (2007) A241–A244.
[17] L. Zhou, et al., Electrochem. Solid-State Lett. 14 (11) (2011) A161–A164.
[18] S.S. Zhang, J. Power Sources 163 (2) (2007) 713–718.
[19] A.A. Granovsky. Firefly Version 7.1.G.
[20] M.W. Schmidt, et al., J. Comput. Chem. 14 (11) (1993) 1347–1363.
[21] T. Kawamura, et al., J. Power Sources 104 (2) (2002) 260–264.
[22] S.E. Sloop, J.B. Kerr, K. Kinoshita, J. Power Sources 119–121 (2003) 330–337.
[23] D. Aurbach, et al., J. Electrochem. Soc. 134 (7) (1987) 1611–1620.
[24] D. Aurbach, et al., J. Electroanal. Chem. 339 (1–2) (1992) 451–471.
[25] M.B. Smith, March's Advanced Organic Chemistry: Reactions, Mechanisms, Structure, John Wiley & Sons, 2013.
[26] H. Ota, et al., J. Electrochem. Soc. 151 (10) (2004) A1659–A1669.
[27] D.P. Abraham, et al., J. Power Sources 180 (1) (2008) 612–620.
[28] Y. Zhu, et al., J. Electrochem. Soc. 159 (12) (2012) A2109–A2117.